East European Journal of Physics. **2.** 252-257 (2025)
DOI:10.26565/2312-4334-2025-2-30 ISSN 2312-4334

THE ROLE OF RECOMBINATION TYPES IN EFFICIENCY LIMITS OF RADIAL p-n JUNCTIONS BASED ON Si AND GaAs

Jo'shqin Sh. Abdullayev[a]*, Ibrokhim B. Sapaev[a,b,d,e], Sardor R. Kadirov[c]
[a]*National Research University TIIAME, Department of Physics and Chemistry, Tashkent, Uzbekistan*
[b]*Western Caspian University, Baku, Azerbaijan*
[c]*Urgench State University, Urgench, Uzbekistan*
[d]*Baku Eurasian University, Baku, AZ 1073, Azerbaijan*
[e]*Central Asian University in Tashkent, Uzbekistan*
**Corresponding Author e-mail: j.sh.abdullayev6@gmail.com*
Received March 1, 2025; revised March 21, 2025; accepted May 13, 2025

In this study, we analyze and model the recombination mechanisms in radial p-n junction structures composed of Si and GaAs over a temperature range of 250 K to 500 K, in 50 K increments. Using both analytical and computational modeling techniques, we examine the effects of doping concentration, core and shell radius, and external voltage on charge carrier behavior and recombination mechanisms. Our analysis focuses on core radii of 0.5 μm and 1 μm, with a total structure height of 4 μm. The external voltage varies from 0 to 2 V, and the doping levels are set to $p = 2\times10^{16}$ cm^{-3} and $n = 2\times10^{17}$ cm^{-3}. A comparative analysis of Si and GaAs highlights their respective advantages in semiconductor applications: Si offers cost-effectiveness and stability, while GaAs exhibits superior electron mobility and radiative recombination efficiency. Additionally, we investigate the influence of external voltage on recombination mechanisms, revealing that GaAs has a higher rate of surface and radiative recombination compared to Si, which is more affected by Auger recombination at high doping levels. These findings provide valuable insights into optimizing material selection for high-performance optoelectronic and photovoltaic devices.
Keywords: *Radial p-n junction; Light trap; External factors; Recombination; Doping concentration; Temperature*
PACS: 73.40. Lq, 73.61.Cw, 73.61.Ey, 72.20.Jv

INTRODUCTION

In recent decades, significant research efforts have focused on developing advanced photovoltaic (PV) architectures to enhance energy conversion efficiency while minimizing fabrication costs. Among the various strategies employed, the integration of micro- and nanostructured materials in radial p-n junction configurations has emerged as a promising approach [1-2]. Compared to conventional planar structures, radial p-n junctions offer several advantages [3-5], including an increased junction area for charge separation [6,7], improved carrier transport due to shorter diffusion lengths [8,9], and enhanced internal and external quantum efficiency [10-12]. Additionally, the orthogonal alignment of light absorption and carrier transport in radial p-n junctions supports high-frequency operation [13,14], making them highly suitable for high-speed electronics [15,16] and wireless communication systems [17].

As a result, radial p-n junctions have been widely adopted in cutting-edge semiconductor technologies, including two-dimensional transistors [18], nanowires, and particularly radial p-n and p-i-n junction structures [19]. Over the past two decades, these junctions have gained increasing attention due to their superior optical and electronic properties, positioning them as ideal candidates for various applications such as photodiodes [20], optical sensors [21], thermal and photovoltaic detectors, and high-efficiency solar cells [22].

Despite their numerous advantages, the efficiency of radial p-n junctions is fundamentally constrained by recombination mechanisms, which play a pivotal role in charge carrier dynamics and overall device performance. However, while recombination processes have been extensively studied in planar and bulk semiconductor structures, their impact in radial p-n junctions remains relatively underexplored. A comprehensive understanding of these recombination pathways is essential for optimizing device efficiency and unlocking the full potential of radial p-n junction-based technologies.

METHODS AND MATERIAL

2.1 Materials and geometric parameters

In this study, we focus on core radii of 0.5 μm and 1 μm within the structure. The height of the structure, as shown in Figure 1, z is 4 μm. The temperature range is considered from 50 K to 500 K in increments of 50 K. An external voltage ranging from 0 to 2 V is applied, and the doping concentrations are set to $p = 2\times10^{16}$ cm^{-3} and $n = 2\times10^{17}$ cm^{-3}. We selected Si and GaAs as the materials for this analysis due to their well-established use in semiconductor devices, this structure has been previously used in our research papers [31]. Si is widely utilized in microelectronics and solar cells because of its abundance, cost-effectiveness, and stable material properties. In contrast, GaAs offers superior electron mobility, direct bandgap properties, and high efficiency in optoelectronic applications such as LEDs, laser diodes, and

Cite as: J.Sh. Abdullayev, I.B. Sapaev, S.R. Kadirov, East Eur. J. Phys. 2, 252 (2025), https://doi.org/10.26565/2312-4334-2025-2-30

high-speed electronics. By comparing these two materials, we aim to evaluate their performance under different structural and temperature conditions. Where r denotes the radial dimension, $+$ and $-$ represents the densities of ionized N_D^+ donor and N_A^- acceptor atoms respectively, at the interface of the radial p-n junction within the depletion region. If full ionization case $N_D^+ = N_D$, $N_A^- = N_A$. In Figure 1 b), the interval $0 < r < r_p$ represents the p-type quasi-neutral region (QNR), the interval $r_p < r < r_n$ represents the depletion region in the radial p-n junction, the interval $r > r_n$ represents the n-type quasi-neutral region (QNR).

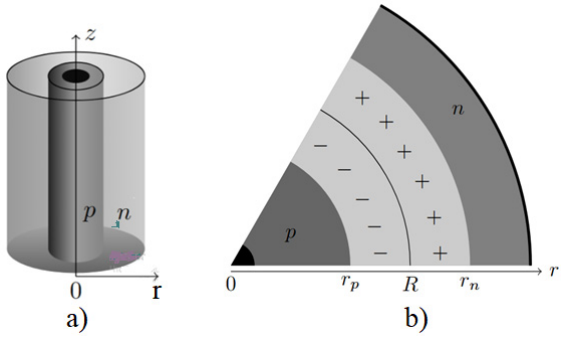

Figure 1. Schematic representation of the radial p-n junction: (a) 3D structure and (b) 2D cross-sectional view

2.2 Recombination models

The radial p-n junction structure has the potential to surpass the Shockley-Queisser limit due to its unique geometric configuration, which enhances charge carrier collection and light absorption compared to conventional planar p-n junctions. However, despite this theoretical advantage, efficiency can be significantly constrained by various recombination mechanisms. These recombination processes, such as Shockley-Read-Hall (SRH) recombination, surface recombination, radiative recombination, and Auger recombination, lead to carrier losses, thereby reducing the actual device performance below the theoretical maximum. A thorough understanding of these recombination pathways is crucial for optimizing the efficiency of radial p-n junction-based optoelectronic and photovoltaic devices.

In this work, we studied the main recombination effects, namely Auger recombination, Shockley-Read-Hall (SRH) recombination in the bulk, surface recombination, and optical generation/radiative recombination. These different recombination effects, along with total recombination, are related as follows (1):

$$R_{Total} = R_{SRH} + R_{Auger} + R_{Rad} + R_{Sur}\,. \tag{1}$$

If we consider $R \sim 1/\tau$, equation (1) can be expressed in terms of the lifetime (τ), obtaining a total effective lifetime (τ_{Total}) as follows (2):

$$\frac{1}{\tau_{Total}} = \underbrace{\frac{1}{\tau_{SRH}} + \frac{1}{\tau_{Auger}} + \frac{1}{\tau_{Rad}}}_{bulk} + \frac{1}{\tau_{Sur}} = \frac{1}{\tau_{bulk}} + \frac{1}{\tau_{Sur}}\,. \tag{2}$$

The carrier lifetime varies depending on the recombination mechanism. Radiative recombination lifetime is inversely proportional to carrier concentration and governed by the radiative recombination coefficient. SRH recombination depends on defect density and carrier capture cross-sections. Auger recombination lifetime decreases with increasing carrier concentration due to carrier-carrier interactions. Surface recombination is influenced by surface recombination velocity and material thickness. Understanding these mechanisms is crucial for optimizing semiconductor device performance. The band gap diagram of a semiconductor, illustrating different recombination mechanisms involving electrons and holes, is shown in Figure 2. Each recombination mechanism is explored in the following subsections. Additionally, the next subsection presents a brief overview of the recombination effects examined in this study, aiming to enhance the comprehension of the obtained results.

Table 1. Comparative Analysis of Si and GaAs in Radial p-n Junctions

Property	Si Radial p-n Junctions	GaAs Radial p-n Junctions
SRH Recombination	Moderate (depends on defects)	High (due to sensitivity to defects)
Auger Recombination	Significant at high doping	More dominant at high injection levels
Radiative Recombination	Negligible	Strong (due to direct bandgap)
Surface Recombination	Moderate	High (due to higher surface recombination velocity)

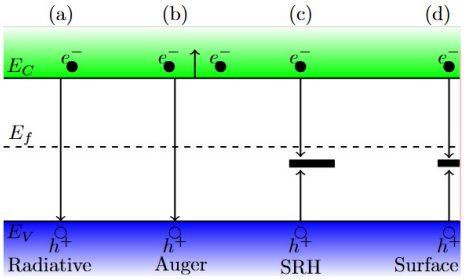

Figure 2. Possible recombination mechanisms in semiconductors include: (a) band-to-band radiative recombination, (b) nonradiative recombination through defect states (SRH recombination), (c) nonradiative Auger recombination, and (d) surface recombination

2.2.1 Shocley-Read-Hall and Surface recombination

In Shockley-Read-Hall (SRH) recombination, a charge carrier transitioning between energy bands is captured by a trap—an energy state introduced by a defect or a dopant. The trapped carrier then releases energy through phonon interactions. This process is predominant in indirect bandgap materials but can also become significant in direct bandgap semiconductors when a high density of traps is present.

For our simulations, we employed the SRH lifetime model, which accounts for concentration-dependent carrier lifetimes since it is also influenced by impurity concentration (Roulston et al., 1982; Law et al., 1991; Fossum and Lee, 1982). Based on this, SRH recombination is described by the following equation (Hall, n.d.):

$$R_{net}^{SRH} = \frac{p \cdot n - \gamma_n \cdot \gamma_p \cdot n_{i,eff}^2}{\tau_p \cdot (n + \gamma_n \cdot n_1) + \tau_n \cdot (p + \gamma_p \cdot p_1)}, \tag{3a}$$

$$R_{Sur,net}^{SRH} = \frac{p \cdot n - n_{i,eff}^2}{\frac{(n+n_1)}{S_p} + \frac{(p+p_1)}{S_n}}. \tag{3b}$$

Where, $\tau_n = 4.4 \cdot 10^{-4}\ s$ and $\tau_n = 2.2 \cdot 10^{-4}\ s$ life time for carrier charge, S_n and S_p surface recombination velocity.

2.2.2 Auger recombination

In this recombination process, an electron and a hole recombine without emitting a photon. Instead, the released energy is transferred to another electron, which is excited to a higher energy level. This excited electron subsequently relaxes back to the conduction band through thermal dissipation (Selberherr, 1984). This model becomes significant at high current densities and elevated carrier concentrations, such as those observed at UH levels. The standard Auger recombination is described by the following equation (Dziewor and Schmid, 1977):

$$R_{net}^{Auger} = (C_n \cdot n + C_p \cdot p)(p \cdot n - n_{i,eff}^2). \tag{4}$$

Where n and p represent the electron and hole concentrations, respectively, $n_{i,eff}$ is the intrinsic concentration, C_n and C_p are the Auger coefficients for electrons and holes, respectively.

2.2.3 Optical generation/radiative recombination

In this mechanism, photon transitions must be considered for generation and recombination processes. It is a direct process because it occurs in a single step. During radiative recombination, an electron loses energy and transitions from the conduction band to the valence band, emitting a photon with energy similar to the bandgap. In optical generation, an electron moves from the valence band to the conduction band. Radiative recombination is the dominant recombination mechanism in direct bandgap materials, such as GaAs, and in narrow-bandgap semiconductors. However, in indirect bandgap materials, this process is very weak and can often be neglected. This model, also known as band-to-band recombination, can be described by equation (5), where the total band-to-band generation/recombination is determined by the difference between the capture rate and the emission rate processes.

$$R_{net}^{Rad} = C_{Rad} \cdot (p \cdot n - n_{i,eff}^2). \tag{5}$$

Where, $C_{Rad} = 1.5 \cdot 10^{-10}\ cm^3 / s$ means the capturerate. The analysis results for each of these recombination effects are presented in Table 1. In all recombinations $n_{i,eff} = 1.5 \cdot 10^{10}\, cm^{-3}$ for Si, $n_{i,eff} = 1.5 \cdot 10^{10}\, cm^{-3}$ for GaAs.

RESULTS AND DISCUSSION

The distribution of recombination rate in the radial direction obtained from the model developed for radial p-n junction structures made of Si and GaAs is presented and analyzed in Figure 3 and Figure 4 in this section. In Figure 3, for R = 0.5 μm, the external voltage is set to 0.2 V and 0.4 V, while the temperature is varied from 250K to 500K in steps of 50K. Thus, the model indicates that in Si material, the recombination process occurs both in the depletion region and the electrically neutral regions, but it is shown to proceed at a higher rate in the depletion region. In contrast, in GaAs material, the recombination rate remains low in the electrically neutral regions $0 < r < r_p$ and $r > r_n$. For radial p-n junctions made of Si and GaAs, the recombination rate is higher in the depletion region $r_p < r < r_n$ for both materials. However, GaAs exhibits a higher maximum recombination rate compared to Si.

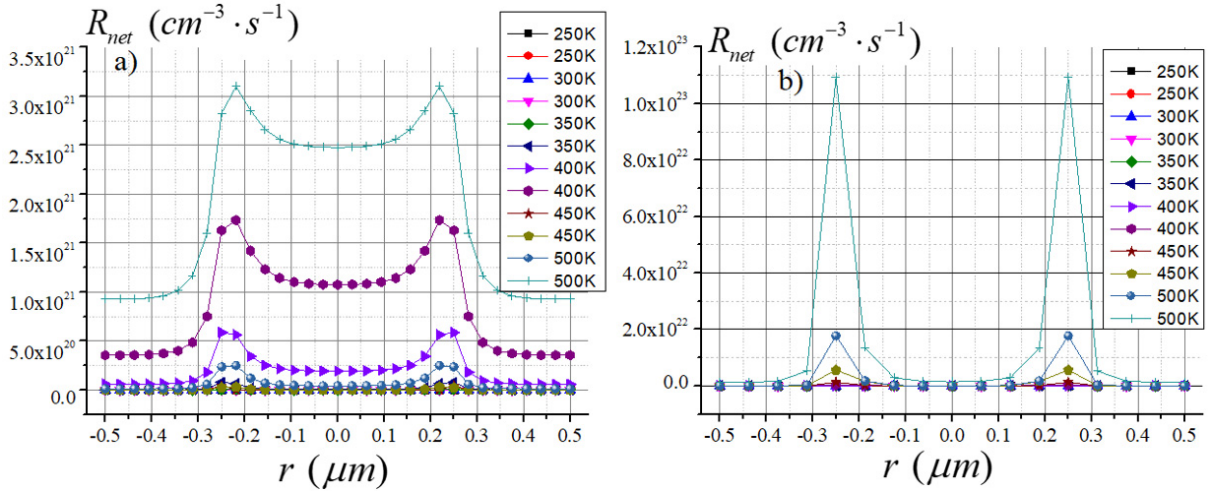

Figure 3. Recombination rate distributions as a function of radial dimension over a temperature range from 250 K to 500 K for (a) Si and (b) GaAs at R=0.5 μm

As the radius decreases, the core region becomes fully depleted, leading to a disruption of internal neutrality. As a result, the recombination rate increases due to the enhanced depletion effect in smaller-radius structures.

In this case, the performance of radial p-n junction structures can vary depending on their application field, as the recombination behavior is strongly influenced by the radius reduction. Figure 4 compares the recombination rates for R = 1 μm in two cases: (a) for Si, (b) for GaAs

The results show that in both materials, the maximum recombination rate decreases as the radius decreases. This suggests that smaller-radius structures exhibit higher recombination rates, while larger-radius structures tend to have lower recombination peak values.

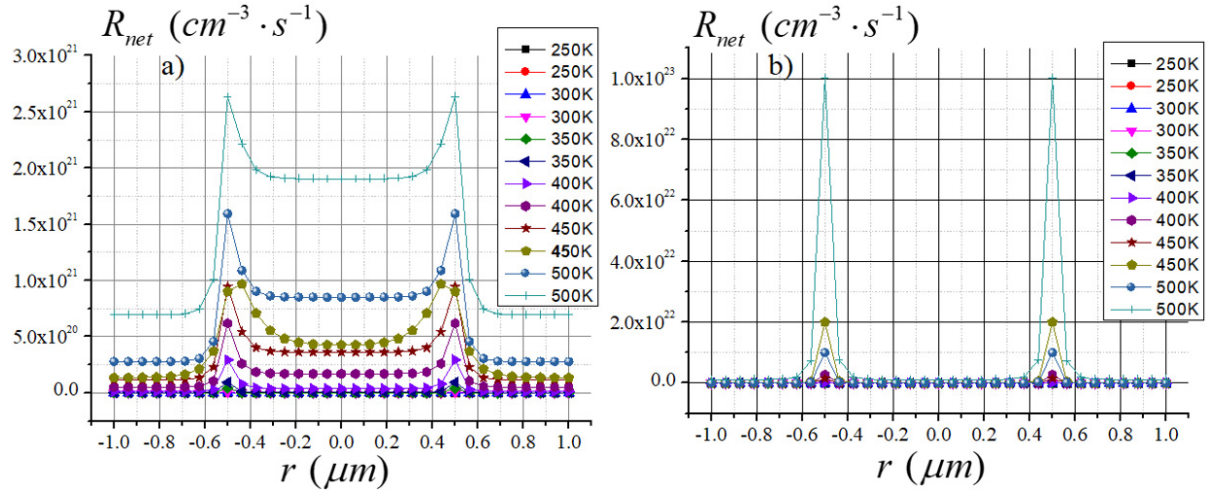

Figure 4. Recombination rate distributions as a function of radial dimension over a temperature range from 250 K to 500 K for (a) Si and (b) GaAs at R=1 μm

The analysis of recombination rate distribution in radial Si and GaAs p-n junction structures reveals the following key points. In Si material, recombination occurs in both the depletion and electrically neutral regions, but it is more dominant in the depletion region. In GaAs material, the recombination rate in the electrically neutral region is lower compared to the depletion region. The depletion region exhibits high recombination rates for both materials, but GaAs

shows a higher peak recombination rate than Si. As the radius decreases, the core region becomes fully depleted, leading to a loss of internal neutrality and an increase in the recombination rate. In Figure 4, for R = 1 μm, the recombination rates for Si and GaAs are compared, showing that as the radius decreases, the maximum recombination rate also decreases. These findings suggest that the performance of radial p-n junction structures depends on the application, as the recombination behavior varies with radius and material properties.

CONCLUSIONS

This study presents a detailed analysis of radial p-n junction structures based on Si and GaAs, emphasizing their distinct electrical and recombination characteristics. The temperature increase from 250 K to 500 K significantly influences charge storage and recombination dynamics, with GaAs exhibiting higher radiative and surface recombination rates due to its direct bandgap and elevated surface recombination velocity. In contrast, Si is more susceptible to Auger recombination at high doping levels. Furthermore, the effects of external voltage on recombination mechanisms underscore the necessity of carefully selecting material and structural parameters for specific semiconductor applications. These findings provide valuable insights for optimizing high-performance optoelectronic and photovoltaic devices, paving the way for advancements in material engineering and device design to enhance efficiency and reliability.

ORCID

Jo'shqin Sh. Abdullayev, https://orcid.org/0000-0001-6110-6616; **Ibrokhim B. Sapaev,** https://orcid.org/0000-0003-2365-1554

REFERENCES

[1] R. Elbersen, R.M. Tiggelaar, A. Milbrat, G. Mul, H. Gardeniers, and J. Huskens, Advanced Energy Materials, **5**(6), 1401745 (2014). https://doi.org/10.1002/aenm.201401745
[2] E. Gnani, A. Gnudi, S. Reggiani, and G. Baccarani, "Theory of the Junctionless Nanowire FET," IEEE Trans. Electron Devices, **58**(9), 2903 (2011). https://doi.org/10.1109/TED.2011.2159608
[3] J.Sh. Abdullayev, and I.B. Sapaev, "Optimization of the Influence of Temperature on The Electrical Distribution of Structures with Radial p-n Junction Structures," East European Journal of Physics, (3), 344-349 (2024). https://doi.org/10.26565/2312-4334-2024-3-39
[4] J.Sh. Abdullayev, and I.B. Sapaev, "Optimizing the Influence of Doping and Temperature on the Electrophysical Features o p-n and p-i-n Junction Structures," Eurasian Physical Technical Journal, **21**(3(49), 21–28 (2024). https://doi.org/10.31489/2024No3/21-28
[5] J.Sh. Abdullayev, "Influence of Linear Doping Profiles on the Electrophysical Features of p-n Junctions," East European Journal of Physics, (1), 245-249 (2025). https://doi.org/10.26565/2312-4334-2025-1-26
[6] O.V. Pylypova, A.A. Evtukh, P.V. Parfenyuk, I.I. Ivanov, I.M. Korobchuk, O.O. Havryliuk, and O.Yu. Semchuk, "Electrical and optical properties of nanowires based solar cell with radial p-n junction," Opto-Electronics Review, **27**(2), 143 (2019). https://doi.org/10.1016/j.opelre.2019.05.003
[7] R. Ragi, R.V.T. da Nobrega, U.R. Duarte, and M.A. Romero, "An Explicit Quantum-Mechanical Compact Model for the I-V Characteristics of Cylindrical Nanowire MOSFETs," IEEE Trans. Nanotechnol. **15**(4), 627 (2016). https://doi.org/10.1109/TNANO.2016.2567323
[8] R.D. Trevisoli, R.T. Doria, M. de Souza, S. Das, I. Ferain, and M.A. Pavanello, "Surface-Potential-Based Drain Current Analytical Model for Triple-Gate Junctionless Nanowire Transistors," IEEE Trans. Electron Devices, **59**(12), 3510 (2012). https://doi.org/10.1109/TED.2012.2219055
[9] N.D. Akhavan, I. Ferain, P. Razavi, R. Yu, and J.-P. Colinge, "Improvement of carrier ballisticity in junctionless nanowire transistors," Appl. Phys. Lett. **98**(10), 103510 (2011). https://doi.org/10.1063/1.3559625
[10] J.Sh. Abdullayev, and I.B. Sapaev, "Modeling and calibration of electrical features of p-n junctions based on Si and GaAs," Physical Sciences and Technology, **11**(3-4), 39–48 (2024). https://doi.org/10.26577/phst2024v11i2b05
[11] J.Sh. Abdullayev, and I.B. Sapaev, "Factors Influencing the Ideality Factor of Semiconductor p-n and p-i-n Junction Structures at Cryogenic Temperatures," East European Journal of Physics, (4), 329-333 (2024). https://doi.org/10.26565/2312-4334-2024-4-37
[12] A.V. Babichev, H. Zhang, P. Lavenus, F.H. Julien, A.Y. Egorov, Y.T. Lin, and M. Tchernycheva, "GaN nanowire ultraviolet photodetector with a graphene transparent contact," Applied Physics Letters, **103**(20), 201103 (2013). https://doi.org/10.1063/1.4829756
[13] D.H.K. Murthy, T. Xu, W.H. Chen, A.J. Houtepen, T.J. Savenije, L.D.A. Siebbeles, *et al*., "Efficient photogeneration of charge carriers in silicon nanowires with a radial doping gradient," Nanotechnology, **22**(31), 315710 (2011). https://doi.org/10.1088/0957-4484/22/31/315710
[14] I. Aberg, G. Vescovi, D. Asoli, U. Naseem, J.P. Gilboy, C. Sundvall, and L. Samuelson, "A GaAs Nanowire Array Solar Cell With 15.3% Efficiency at 1 Sun," IEEE Journal of Photovoltaics, **6**(1), 185 (2016). https://doi.org/10.1109/JPHOTOV.2015.2484967
[15] J. Sh. Abdullayev, I. B. Sapaev, and Kh. N. Juraev, "Theoretical analysis of incomplete ionization on the electrical behavior of radial p-n junction structures," Low Temp. Phys. **51**, 60–64 (2025). (https://doi.org/10.1063/10.0034646)
[16] J.Sh. Abdullayev, and I.B. Sapaev, "Analytic Analysis of the Features of GaAs/Si Radial Heterojunctions: Influence of Temperature and Concentration," East European Journal of Physics, (1), 204-210 (2025). https://doi.org/10.26565/2312-4334-2025-1-21
[17] O. Toktarbaiuly, M. Baisariyev, A. Kaisha, T. Duisebayev, N. Ibrayev, T. Serikov, M. Ibraimov, *et al*., "Enhancement of Power Conversion Efficiency of Dye-Sensitized Solar Cells Via Incorporation of Gan Semiconductor Material Synthesized in Hot-Wall Chemical Vapor Deposition Furnace," Eurasian Physical Technical Journal, **21**(4(50), 131–139 (2024). https://doi.org/10.31489/2024No4/131-139
[18] M.Sh. Isaev, A.I. Khudayberdieva, M.N. Mamatkulov, U.T. Asatov, and S.R. Kodirov, "The Surface Layer Morphology of Si<Cr> Samples," East European Journal of Physics, (4), 297–300 (2024). https://doi.org/10.26565/2312-4334-2024-4-32

[19] I. Sapaev, I.B. Sapaev, *et. al*., E3S Web Conf. **383**, 04022 (2023). https://doi.org/10.1051/e3sconf/202338304022
[20] A.T. Mamadalimov, M.Sh. Isaev, M.N. Mamatkulov, S.R. Kodirov, and J.T. Abdurazzokov, "Study Of Silicide Formation In Large Diameter Monocrystalline Silicon," East European Journal of Physics, (2), 366–371 (2024). https://doi.org/10.26565/2312-4334-2024-2-45
[21] M.S. Isaev, U.T. Asatov, M.A. Tulametov, S.R. Kodirov, and A.E. Rajabov, "Study of The Inhomogeneities of Overcompensed Silicon Samples Doped with Manganese," East European Journal of Physics, (2), 341–344 (2024). https://doi.org/10.26565/2312-4334-2024-2-40
[22] B. Pal, K.J. Sarkar, and P. Banerji, Solar Energy Materials and Solar Cells, **204**, 110217 (2020). https://doi.org/10.1016/j.solmat.2019.110217

РОЛЬ ТИПІВ РЕКОМБІНАЦІЇ У МЕЖАХ ЕФЕКТИВНОСТІ РАДІАЛЬНИХ p-n ПЕРЕХОДІВ НА ОСНОВІ Si ТА GaAs

Джошкін Ш. Абдуллаєв[a], Іброхім Б. Сапаєв[a,b,d,f], Сардор Р. Кадиров[c]
[a]Національний дослідницький університет ТІІАМЕ, кафедра фізики та хімії, Ташкент, Узбекистан
[b]Західно-Каспійський університет, Баку, Азербайджан
[c]Ургенчський державний університет, Ургенч, Узбекистан
[d]Бакинський Євразійський університет, Баку, Аризона 1073, Азербайджан
[e]Центральноазіатський університет у Ташкенті, Узбекистан

У цьому дослідженні ми аналізуємо та моделюємо механізми рекомбінації в радіальних p-n переходах, що складаються з Si та GaAs, у температурному діапазоні від 250 K до 500 K з кроком 50 K. Використовуючи як аналітичне, так і комп'ютерне моделювання, ми вивчаємо вплив концентрації домішок, радіусу ядра та оболонки, а також зовнішньої напруги на поведінку носіїв заряду та механізми рекомбінації. Наш аналіз фокусується на радіусах ядра 0,5 мкм і 1 мкм, при загальній висоті структури 4 мкм. Зовнішня напруга варіюється від 0 до 2 В, а рівні легування встановлені як $p = 2\times10^{16}$ см$^{-3}$ і $n = 2\times10^{17}$ см$^{-3}$. Порівняльний аналіз Si та GaAs висвітлює їхні відповідні переваги в напівпровідникових застосуваннях: Si забезпечує економічність і стабільність, тоді як GaAs демонструє кращу рухливість електронів і високу ефективність радіаційної рекомбінації. Додатково, ми досліджуємо вплив зовнішньої напруги на механізми рекомбінації, виявляючи, що GaAs має вищу швидкість поверхневої та радіаційної рекомбінації, тоді як Si більше схильний до Оже-рекомбінації при високих рівнях легування. Отримані результати надають цінну інформацію для оптимізації вибору матеріалів у високоефективних оптоелектронних і фотоелектричних пристроях.

Ключові слова: *радіальний p-n перехід; світлова пастка; зовнішні фактори; рекомбінація; концентрація домішок; температура*